J Membrane Biol (2015) 248:837–847
DOI 10.1007/s00232-015-9788-7

Picosecond and Terahertz Perturbation of Interfacial Water and Electropermeabilization of Biological Membranes

P. Thomas Vernier[1] · Zachary A. Levine[2,3] · Ming-Chak Ho[4] · Shu Xiao[1] · Iurii Semenov[1] · Andrei G. Pakhomov[1]

Received: 13 January 2015 / Accepted: 10 March 2015 / Published online: 22 March 2015

Abstract Non-thermal probing and stimulation with subnanosecond electric pulses and terahertz electromagnetic radiation may lead to new, minimally invasive diagnostic and therapeutic procedures and to methods for remote monitoring and analysis of biological systems, including plants, animals, and humans. To effectively engineer these still-emerging tools, we need an understanding of the biophysical mechanisms underlying the responses that have been reported to these novel stimuli. We show here that subnanosecond ($\leq$500 ps) electric pulses induce action potentials in neurons and cause calcium transients in neuroblastoma-glioma hybrid cells, and we report complementary molecular dynamics simulations of phospholipid bilayers in electric fields in which membrane permeabilization occurs in less than 1 ns. Water dipoles in the interior of these model membranes respond in less than 1 ps to permeabilizing electric potentials by aligning in the direction of the field, and they re-orient at terahertz frequencies to field reversals. The mechanism for subnanosecond lipid electropore formation is similar to that observed on longer time scales—energy-minimizing intrusions of interfacial water into the membrane interior and subsequent reorganization of the bilayer into hydrophilic, conductive structures.

Keywords Electropermeabilization · Electroporation · Molecular dynamics · Picosecond · Terahertz · Water bridge

✉ P. Thomas Vernier
pvernier@odu.edu

[1] Frank Reidy Research Center for Bioelectrics, Old Dominion University, 4211 Monarch Way, Norfolk, VA 23508, USA

[2] Department of Physics, University of California Santa Barbara, Santa Barbara, CA, USA

[3] Department of Chemistry and Biochemistry, University of California Santa Barbara, Santa Barbara, CA, USA

[4] Department of Physics and Astronomy, University of Southern California, Los Angeles, CA, USA

Introduction

In recent years, investigations of the effects of ultra-short electric pulses on biological systems have probed shorter and shorter time scales, reaching now even into the picosecond range (Schoenbach et al. 2008; Xiao et al. 2011; Camp et al. 2012). Because picosecond electric pulses have very fast rise times, they contain significant amounts of energy in the gigahertz and terahertz spectral regions, and we note that on this separate track studies of biological responses to terahertz electromagnetic radiation (with picosecond polarity reversals) have also expanded over the past few years, as terahertz sources have become more accessible. Some investigators report no effects of terahertz exposures (Zeni et al. 2007; Williams et al. 2013; Hintzsche et al. 2013). Where responses are observed (Ramundo-Orlando and Gallerano 2009), some appear to be associated with temperature increases (Wilmink et al. 2011), but others seem to be caused by direct, temperature-independent interactions of electric fields with biological processes (Titova et al. 2013a, b). Millimeter waves, an electromagnetic regime that may be considered to overlap with terahertz radiation, have also been reported to affect biological systems (Ramundo-Orlando et al. 2007; Kim et al. 2013; Albini et al. 2014; Romanenko et al. 2014), and these phenomena may be related. Because effects from both picosecond pulses and terahertz radiation imply

electric-field-driven biomolecular rearrangements on the picosecond time scale, the mechanisms for the two sets of phenomena are likely to be related, and it may be beneficial to consider them together.

Apart from the functional stimulation of electrically active cells, the most reproducible, least ambiguous, and best understood non-thermal bio-effect of pulsed electric fields is the permeabilization of membranes, a process called electroporation or electropermeabilization (Teissie and Rols 1993; Rols 2006). In the presence of an external electric field of sufficient magnitude and duration, permeabilizing structures form in cell membranes, breaching the normal barrier function, and permitting the transport of normally impermeant materials into or out of the cell (Neumann et al. 1982; Marty et al. 2006; Heller and Heller 2006; Frandsen et al. 2012).

Most electroporation protocols for laboratory, clinical, and biotechnological applications use pulses with durations of at least 100 μs, but membrane permeabilization occurs with pulses shorter than 100 ns (Pakhomov et al. 2007a) or even 10 ns (Benz and Zimmermann 1980; Vernier et al. 2006a). Permeabilization of cell membranes with submicrosecond pulsed electric fields is accompanied by a host of other effects, many of which are consequences of the initial breaching of membrane integrity observed not only for the plasma membrane but also for intracellular, membrane-bound structures (Schoenbach et al. 2001; Vernier et al. 2003, 2004; Tekle et al. 2005; Nuccitelli et al. 2006; Pakhomov et al. 2007b; Craviso et al. 2010; Napotnik et al. 2010, 2012 Ibey et al. 2011; Pakhomova et al. 2012; Silve et al. 2012; Tolstykh et al. 2014).

"Long-pulse" (>100 ns) electroporation models treat the membrane as a capacitor which is charged by ions migrating in the applied electric field until a critical transmembrane potential is reached and permeabilizing structures are formed (Coster 1965; Zimmermann et al. 1974; Abidor et al. 1979; Sugar and Neumann 1984; Weaver and Chizmadzhev 1996; Neu and Krassowska 1999). As the pulse duration (the time during which the membrane is charged) is reduced, higher and higher fields are needed for detectable permeabilization (Vernier et al. 2006a; Ibey et al. 2010). For very short pulses (<10 ns), however, if the field is high enough (>1 MV/m), a porating field develops across the membrane from dielectric effects alone, and the contribution of charge migration to the permeabilization process becomes less significant (Kotnik and Miklavcic 2000; Gowrishankar and Weaver 2003; Timoshkin et al. 2006).

In one report, subnanosecond pulses of 800 ps duration produced membrane permeabilization at physiological temperatures only after exposures that involved either very large numbers (hundreds) of pulses or very high external fields (>10 MV/m) (Schoenbach et al. 2008). Permeabilization with 200 ps pulses requires even stronger doses—thousands of pulses when the field is 25 MV/m (Xiao et al. 2011). Interestingly, fields greater than 10 MV/m are reported to produce non-thermal effects from exposures of cells to terahertz electromagnetic fields (EMF) (Wilmink et al. 2011; Titova et al. 2013b).

The mechanism for the permeabilizing restructuring of the membrane that occurs in all of these regimes remains an open question (Teissie et al. 2005). Molecular dynamics simulations provide a view of one type of permeabilizing structure, the lipid electropore (Tieleman 2004; Gurtovenko and Vattulainen 2005; Tarek 2005; Böckmann et al. 2008; Levine and Vernier 2010), consistent with experimental observations (Melikov et al. 2001; Naumowicz and Figaszewski 2013; Koronkiewicz et al. 2002), and continuum models (Zimmermann et al. 1974; Abidor et al. 1979; Chizmadzhev and Abidor 1980; Weaver and Chizmadzhev 1996). The formation of these nanometer-scale, conductive pores is initiated by the electric-field-stabilized intrusion of interfacial water into the membrane interior, which leads to the construction of energy-minimized water bridges across the lipid bilayer and the reorganization of the membrane phospholipids along the water columns to form the hydrophilic wall of the pore (Tokman et al. 2013). Although lipid electropores are only one component of the electropermeabilized cell membrane, they are the first structures to form after the application of a porating electric field, and it may be that for very short pulses or very high-frequency EMF they are the dominant structures.

Lipid electropore formation is a stochastic process, with the probability of a pore forming at a given location increasing as an exponential function of the transmembrane electric field (Sugar and Neumann 1984; Vernier et al. 2013). This means that fewer pores form at lower fields, at lower areal densities. Once the process is initiated at a given locus; however, construction of a hydrophilic, conductive pore is complete within a nanosecond—less than a nanosecond at higher fields (Levine and Vernier 2010). Continuum and molecular models, then, are consistent with the formation of electropores on the picosecond time scale.

Experimental studies of biological systems exposed to electric fields at gigahertz and terahertz frequencies or picosecond pulse durations are challenging from an engineering point of view (parasitic impedances which can be neglected for slower signals must be taken into account), but are essential for validating the models. Here we report recent experimental results and new molecular simulation results that together shed new light on the biophysical initiating steps that lead to such profound disruptions "downstream"—osmotic stress, redistribution of membrane phospholipids, and cell death by apoptosis or other pathways.

Methods

Cell Culture

NG108 rat neuroblastoma-glioma hybrid cells (ATCC HB-12317) cells were cultured at 37 °C with 5 % CO_2 in air in Dulbecco's Modified Eagle's medium (Caisson Labs, North Logan, UT) without sodium pyruvate, supplemented with 4 mM L-glutamine, 4.5 g/L glucose, 10 % FBS, 0.2 mM hypoxanthine, 400 nM aminopterin, and 0.016 mM thymidine (without antibiotics). Media supplements were from Sigma-Aldrich (St. Louis, MO) except for the FBS (Atlanta Biologicals, Norcross, GA). For the passage immediately preceding experiments, cells were transferred onto glass coverslips. Primary rat hippocampus neurons were obtained from Life Technologies (Carlsbad, CA) and seeded on poly-D-lysine/laminin-coated coverslips (BD Bioscience, Bedford, MA). The neurons were grown at 37 °C with 5 % CO_2 in air in the supplier-recommended medium (Neurobasal medium supplemented with 200 mM GlutaMAX I and 2 % of B27, all from Life Technologies).

Calcium Imaging

Procedures for loading cells with Fura-2, calibration of the dye, and time-lapse fluorescence imaging were reported previously (Semenov et al. 2013). Briefly, to load the dye, cells on coverslips were incubated for 30 min in physiological buffer (in mM: 140 NaCl, 5.4 KCl, 1.5 $MgCl_2$, 2 $CaCl_2$, 10 glucose, and 10 HEPES, pH 7.2, ~300 mOsm/kg) containing 5 μM Fura-2/AM and 0.02 % Pluronic F-127 (Life Technologies, Grand Island, NY), in the dark at room temperature. Then the coverslips were rinsed in buffer without dye and detergent for 15 min and transferred to a glass-bottomed perfusion chamber (Warner Instruments, Hamden, CT) mounted on an Olympus IX71 inverted microscope (Olympus America, Center Valley, PA).

Dual excitation at 340 and 380 nm for ratiometric imaging was carried out with a Lambda DG4 wavelength switching system (Sutter Instruments, Novato, CA), with emission measured at 510 nm every 150 ms (20 ms exposure at each wavelength) using a C9100-02 EM CCD camera (Hamamatsu Photonics, Japan). The cytosolic-free calcium concentration ($[Ca^{2+}]_i$) was calculated from the Fura-2 emission ratio with a help of Metafluor v.7.5 software (Molecular Devices, Sunnyvale, CA). $[Ca^{2+}]_i$ measurements typically began 1 min prior to electric pulse application. In most experiments, fluorescence intensity traces were smoothed with an Origin 8.0 FFT filter utility (OriginLab Corporation Northampton, MA).

Pulse Generator and Delivery System

Generation of picosecond pulses with an FPG 20-1 pulse generator (FID GmbH, Burbach, Germany) and delivery of the pulses to cells on the stage of an epifluorescence microscope were carried out using methods similar to those previously described (Xiao et al. 2011). For the hippocampal neuron experiments, a micro-coaxial cable (outer diameter 310 μm, inner diameter 80 μm), with insulation removed from the last 350 μm to expose the inner conductor, was used to deliver pulses to the cells. The end of the cable was positioned over the cells with a micromanipulator (Fig. 1). The electric field distribution was simulated by a 3-D electric field solver, Amaze (Field Precision, Albuquerque, NM) (Fig. 1). To avoid blockage of the image by the coaxial cable tip, we chose the two regions near the tip, indicated by the circles. The electric field for these two regions is about 5 MV/m. For this micro-coaxial electrode configuration, the pulse width was about 320 ps (full-width, half-maximum).

For experiments with NG108 neuroblastoma-glioma hybrid cells, pulses were delivered to cells in the bath by means of a pair of tungsten rods (100 μm diameter, 170 μm gap, 3.5 mm long) at the end of a 50 Ω RG316 coaxial cable. The connection is secured with epoxy, which also prevents air breakdown between the rods. Arcing does not occur when the rods are submerged into the aqueous medium covering the cells. The electrode assembly was positioned with an MPC-200 robotic manipulator (Sutter Instruments, Novato, CA) that placed the tips of the rods at

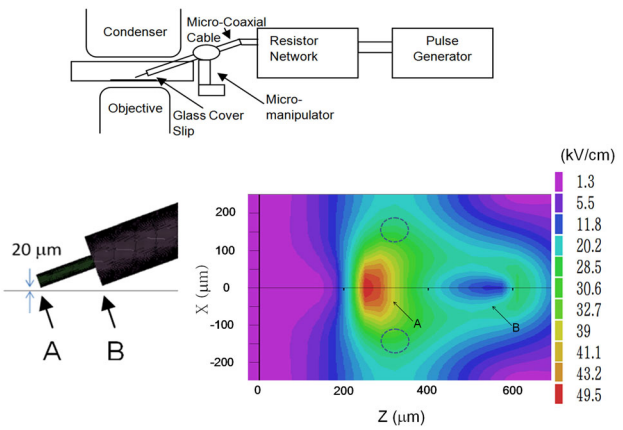

Fig. 1 Micro-coaxial cable pulse delivery system for neurons on microscope stage. The tip of the micro-coaxial cable (the inner conductor) is 20 μm above the cover slip. Regions A and B are projections of the micro-coaxial cable. Cells to be analyzed are within the two off-axis *dashed ellipses*. The *color* map shows the electric field distribution at the surface of the coverslip for a 1 kV pulse voltage, in which case the electric field in the elliptical areas is about 3 MV/m (Color figure online)

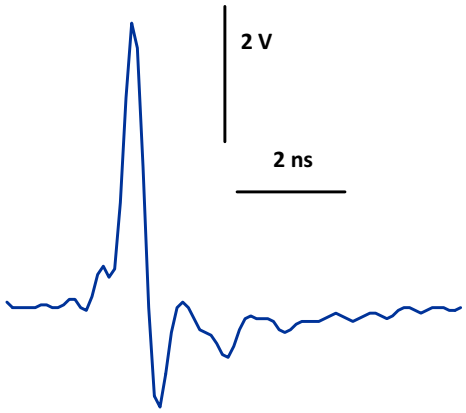

Fig. 2 Picosecond pulse waveform at the output of the pulse generator. 320 ps (full-width, half-maximum), 5.5 kV

precisely 50 μm above the coverslip surface with selected cells being in the middle of the gap between the tips. For this parallel rod electrode configuration, some pulse broadening was observed in simulations, to about 500 ps, but the electric field was 19 MV/m, higher than that in the coaxial electrode configuration.

Pulses were triggered externally and synchronized with image acquisitions by a TTL pulse protocol using a Digidata 1440A board and Clampex v. 10.2 software (Molecular Devices). Timing of pulse delivery, pulse repetition interval, and the number of pulses were all programmed in Clampex. A typical pulse waveform is shown in Fig. 2.

Patch Clamp

Whole-cell measurements of plasma membrane potential were performed in current-clamp mode using a Multiclamp 700B amplifier, Digidata 1322A A–D converter, and pCLAMP software (Molecular Devices). For imaging, a coverslip with attached cells was placed into a glass-bottomed chamber on an Olympus IX81/FV1000 confocal laser scanning system. Bath and pipette buffers contained, respectively, (in mM): 136 NaCl, 5 KCl, 2 $MgCl_2$, 2 $CaCl_2$, 10 HEPES, and 10 glucose (pH 7.4) and 150 K gluconate, 10 NaCl, 5 K-EGTA, 1 $MgCl_2$, 1 $CaCl_2$, and 10 HEPES (pH 7.2).

Molecular Dynamics Simulations

Simulations were performed using GROMACS version 4.0.5 (Hess et al. 2008) on the University of Southern California High Performance Computing and Communications (HPCC) Linux cluster (http://www.usc.edu/hpcc/). Lipid topologies, water model, thermostat, barostat, bond constraints, equilibration protocols, calculation of electrostatic interactions, and other parameters and procedures were as previously described (Ho et al. 2013). Simulations were run at 310 K in the NPT ensemble. Lipid bilayers are composed of 128 POPC lipids (64 per leaflet) and at least 35 waters/lipid (some systems had 70 waters/lipid; this had no effect on the outcome), with initial system dimensions of approximately 7 nm × 7 nm × 7 nm (10 nm for the systems containing more water). The planes of the water–lipid interface are normal to the z-direction of the simulation box. The electric field is always applied along the z-axis, normal to the plane of the bilayer. Molecular graphics images were generated with Visual Molecular Dynamics (VMD) (Humphrey et al. 1996).

Results and Discussion

Subnanosecond Pulse-Induced Activation of Neurons

Fewer than 50, 320 ps, and 5 MV/m pulses are sufficient to activate a hippocampal neuron (Fig. 3, −100 pA trace). Although the exploratory experiments reported here were not designed to determine the pulse-number dose response, we can see that when a current-clamped cell is just slightly depolarized with a 20-pA step, the action potential appears even more quickly, after fewer than 10 pulses (Fig. 3,

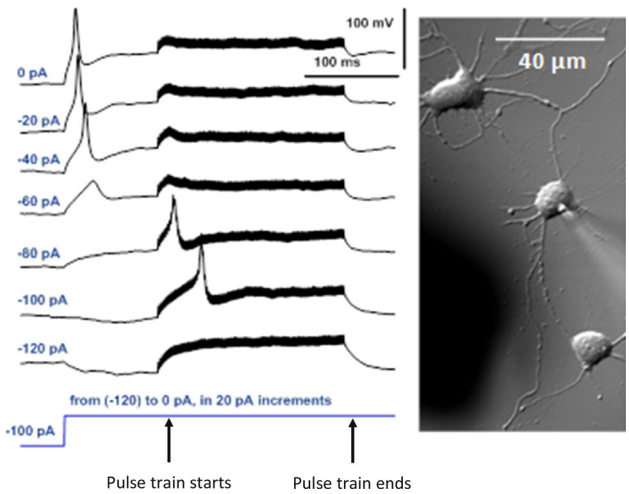

Fig. 3 Action potentials in a rat hippocampal neuron stimulated by 320 ps electric pulses. Membrane voltage in whole-cell configuration measured in current-clamp mode with current stepped in 20 pA increments from the holding level of −100 pA, vertically separated for clarity. Current protocol shown below voltage traces. 100 ms after each current step (*arrow*), 100 pulses, 5 MV/m, 500 Hz) were delivered over a period of 200 ms. Pulse-induced depolarization and action potentials occurred at the −100 and −80 pA steps. Further depolarization by reducing the injected current immediately caused an action potential followed by a refractory state, so the picosecond pulses produced some additional depolarization without eliciting an action potential. The *inset* shows the neuron with a recording pipette attached in the vicinity of the pulse-delivering electrode (*shadow*) (Color figure online)

−80 pA trace). Further depolarization causes an immediate action potential (before pulse delivery) followed by a refractory state. In these conditions picosecond pulses result in further depolarization but no action potential (Fig. 3, traces for 0 pA, −20, −40, −60 pA).

Subnanosecond Pulse-Induced Calcium Transients in Neuroblastoma Cells

A single 500 ps, 19 MV/m pulse causes an immediate 10 nM increase (small but detectable) in intracellular Ca^{2+} concentration in NG108 rat neuroblastoma-glioma hybrid cells (Fig. 4). This $[Ca^{2+}]_i$ increase is dose dependent. A five-pulse exposure (pulse repetition rate = 1 kHz) increases $[Ca^{2+}]_i$ about five times as much as one pulse (Fig. 4). For a single pulse, higher pulse amplitudes (up to 30 MV/m) cause larger increases in $[Ca^{2+}]_i$ (data not shown). Cytosolic calcium levels remain elevated for at least 100 s after a single 500 ps pulse.

Subnanosecond Electropore Formation in Molecular Simulations of POPC Bilayers

In order to see what restructuring of the membrane might occur on a subnanosecond time scale, we carried out MD simulations of POPC bilayers in high electric fields. With applied fields greater than 1.5 GV/m, lipid electropore formation occurs in less than 1 ns (Fig. 5). The pore construction process is similar to that observed with lower fields (Levine and Vernier 2010). In some simulations a pore appears in less than 50 ps. This is not surprising, since it is known that lipid electropore initiation is a stochastic event and that pore initiation time is an exponential function of the electric field (Vernier et al. 2006b; Bockmann et al. 2008).

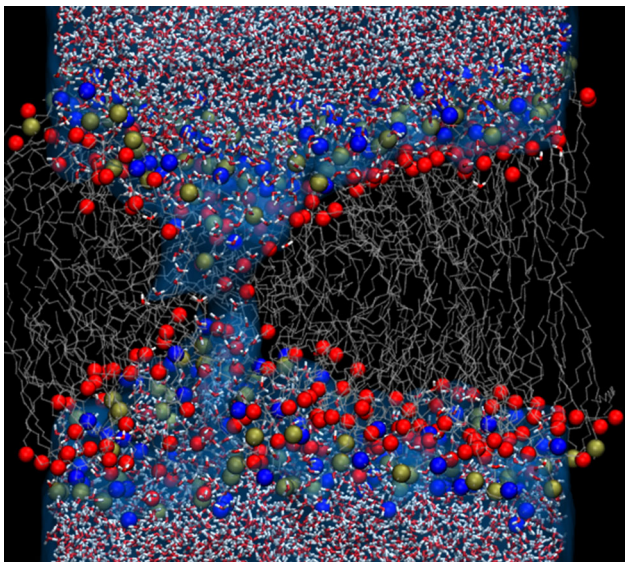

Fig. 5 Lipid electropore in POPC bilayer forms in less than 1 ns. In this high applied electric field (E_{vacuum} = 2.5 GV/m; $E_{effective}$ = 12.5 MV/m), pore initiation is rapid and a hydrophilic pore is constructed in less than 1 ns. Water molecules (*small red* and *white* structures) penetrate the membrane interface and bridge the membrane interior, followed by the phospholipid head groups (*blue*-nitrogen; *gold*—phosphorus; *red*—backbone acyl oxygen). *Gray* strands are the lipid hydrocarbon tails (Color figure online)

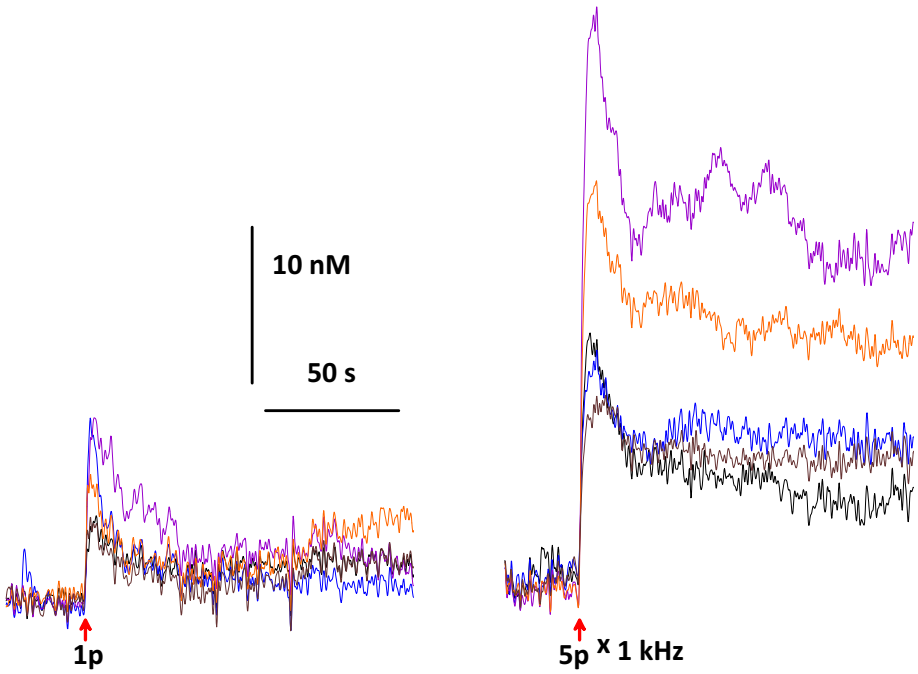

Fig. 4 Ca^{2+} transients in NG108 rat neuroblastoma-glioma hybrid cells evoked by a single 500 ps, 19 MV/m pulse, and a train of 5 pulses at 1 kHz. Measured with Fura-2 ratiometric imaging. Traces from 5 cells superimposed in each *panel*

It should be kept in mind that in an aqueous system the magnitude of the effective electric field is determined in part by the dielectric permittivity of water. At low frequencies, the effective field is approximately 1/80 the value of the "applied" (vacuum) field, which means that the field delivered by the pulse generator in an equivalent experimental system will be approximately 1/80 of the value of the external ("vacuum") field specified in a simulation. For 1.5 GV/m in a simulation, for example, the corresponding field in an experiment (electrode voltage divided by electrode separation for a parallel plate configuration) would be approximately 19 MV/m, within the range required for bioelectric effects with "few nanosecond" and picosecond pulses, and similar to the field used in the experiments reported here.

The actual conditions of both our experiments and our simulations, however, are more complicated. First, we are working at frequencies or on time scales where the relative dielectric permittivity of water is much less than 80 (Barthel et al. 1990). Second, the intrusion of individual water molecules from the complex dielectric landscape of the membrane interface to the low-permittivity environment of the lipid bilayer interior is a phenomenon much better treated in atomic detail, where macroscale material properties like permittivity are of limited utility (Tokman et al. 2013).

Subnanosecond Lipid Bilayer Perturbation with Picosecond (Terahertz) Alternating Electric Fields

With these same porating electric fields, water intrusion and permeabilization of POPC bilayers occurs within tens of picoseconds even when the polarity of the applied electric field is reversed every picosecond (Fig. 6), a terahertz repetition rate. What we observe under these alternating field conditions; however, rather than the typical formation of a single lipid pore that we see when a non-varying electric field is applied to our very small simulated area (50 nm^2), is a more general disorganization of the bilayer, with numerous individual water bridges instead of one or two, even in this small area, and a more scattered, less determinate distribution of phospholipid head groups across the bilayer interior. Instead of a discrete pore we see a scrambled, disordered mixture of water and phospholipid.

Intuitively we might expect that each picosecond reversal of the electric field direction would "undo" whatever rearrangement had occurred in the preceding cycle, with no net effect. In addition, since the textbook water dipole relaxation time is on the order of 8 ps (Buchner et al. 1999), we might think that water molecule orientation should not be appreciably affected by symmetrical electric field reversals occurring at 1 ps intervals. Finally, interactions of water dipoles with phospholipid head groups retards the reorientation of interfacial water in an applied electric field (Pal et al. 2004; Tielrooij et al. 2009). What happens in the simulations is contrary to these expectations. The stabilization of intruding interfacial water by the applied electric field (Tokman et al. 2013) is not reversed when the field direction changes. The water bridges grow, rather than shrink, cycle after cycle, drawing the phospholipid head groups after them.

A closer look reveals how this can be. Note the orientation of the water molecules in the low-permittivity bilayer interior in the two panels of Fig. 7. They rotate to align with the alternating electric field in less than 1 ps. Since there is no hydrogen-bonded network in this local environment to constrain the motion of individual water molecules, the effective relaxation time is much less than it is in bulk water. Water dipole rotation is *retarded* by interactions with interfacial lipids and proteins (Sterpone et al. 2006), but the isolated water molecules that stack up

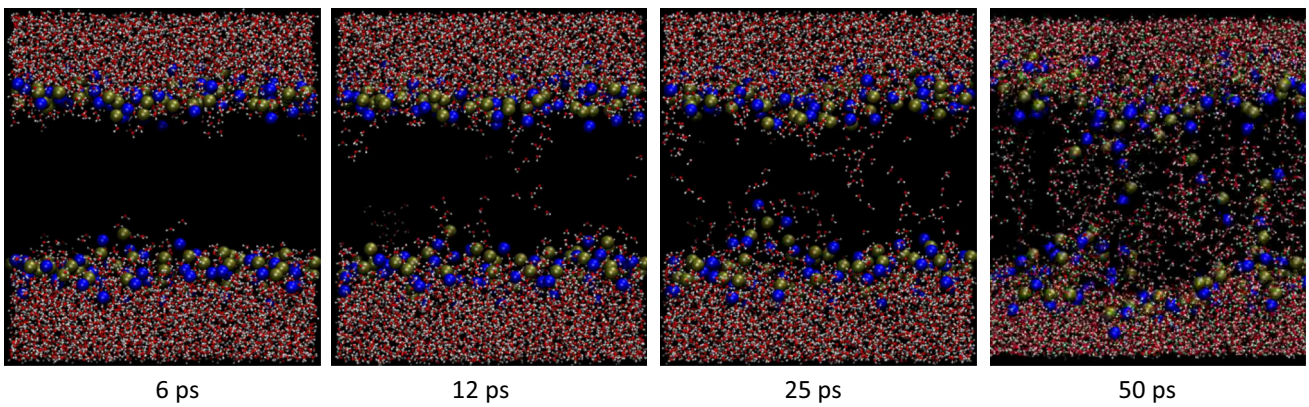

Fig. 6 Permeabilization of POPC bilayer in 500 GHz alternating electric field. Water, then phospholipid head groups bridge the membrane interior in a very high porating electric field with polarity reversals every picosecond. Multiple water bridges appear, followed by head groups, in a few tens of picoseconds

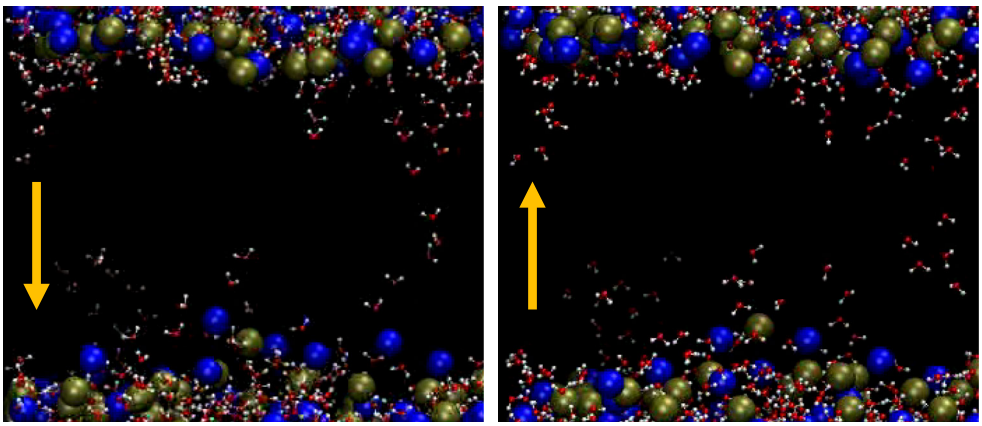

Fig. 7 Dipole reversal for water molecules in the phospholipid bilayer interior. Note that the oxygen (*red*) end of each of the bridging water molecules in the *middle* of the membrane is positioned toward the *bottom* of the *left* image and toward the *top* of the *right* image. The electric field direction is opposite in these two frames, which are 1 ps apart. Within that 1 ps the water dipoles in the membrane interior align in the new field direction. Dipole relaxation time for water in the membrane interior is much less than in bulk water, so that field-stabilized intruding water columns remain the lower energy configuration for interfacial water (Color figure online)

in the membrane interior during pore initiation have escaped their interfacial associations. A field-stabilized water column penetrating the membrane remains a lower energy configuration for interfacial water than the planar lipid-water junction of an unperturbed bilayer regardless of the 180-degree flips of the individual molecules making up the structures.

These simulations provide a plausible mechanism for the permeabilizing restructuring of biological membranes by subnanosecond electric pulses and by rapidly alternating electric fields, even into the terahertz spectral range.

Reconciliation of Experimental Observations of Cellular Responses to Subnanosecond Pulse Exposures with Molecular Simulations of Phospholipid Bilayers in Strong, Rapidly Changing Electric Fields

Although other interpretations are possible, the experimental data presented here are consistent with cell membrane permeabilization by subnanosecond electric pulses, with subsequent depolarization of neurons through the discharge of ion concentration gradients and the triggering of an action potential. This subnanosecond electropermeabilization, however, seems different from those seen after exposure to somewhat longer pulses—600 or 60 ns. Specifically, the permeabilizing structures associated with the subnanosecond electroporation reported here (Fig. 3) appear to seal (membrane conductance recovers) much faster (within 20 ms) than those observed after 600 ns (Fig. 1 in Pakhomov et al. 2009) or 60 ns (Fig. 2 in Ibey et al. 2010) pulse exposure, where membrane conductance remained low for 60 s or more.

Membrane Depolarization by Ion Transport Through Lipid Electropores

Simulations and experimental evidence indicate that transmembrane electric fields can cause the formation of membrane pores with diameters on the order of 1–2 nm (Gurtovenko and Vattulainen 2007; Marrink et al. 2009; Nesin et al. 2010; Romeo et al. 2013) and that the time for pore formation, an exponential function of the applied electric field, can be less than a nanosecond (Levine and Vernier 2010). Molecular simulations of ion transport through lipid electropores have shown that the electrical conductance of these pores is comparable to the conductance of lipid pores determined experimentally (Ho et al. 2013). It seems reasonable to consider whether ion transport through nanoscale lipid electropores formed by nanosecond or subnanosecond electric pulse exposure could be sufficient to depolarize the cell membrane.

For a spherical cell with radius 10 μm, assuming a membrane capacitance of 1×10^{-2} F m^{-2}, an imbalance of 8×10^6 integral charges (monovalent ions) will create a transmembrane potential of 100 mV. This potential can be discharged (depolarizing the cell membrane) by transporting 8×10^6 positive or negative ions into or out of the cell, as appropriate, depending on the polarities chosen. Normally the potential inside the cell is negative with reference to the extracellular medium, so we could discharge −100 mV, for example, by transporting 8×10^6 Na^+ from the medium into the cell.

Neglecting the relatively small electrophoretic transport of ions through pores while the field is applied (because the pulse duration is so short), and considering only diffusive transport through pores remaining after the pulse, we can

estimate the rate of diffusion through a lipid electropore by assuming a simple pore geometry and using the approximate method of (Hille 2001). For $[Na^+] = 150$ mM, $r_{pore} = 1$ nm, $D_{Na+} = 1.33 \times 10^{-9}$ m^2 s^{-1}, $l_{pore} = 5$ nm, we obtain a diffusion transport rate of 5.7×10^7 Na^+ s^{-1} for a single pore. At that rate a single lipid electropore will transport enough Na^+ to depolarize the membrane in less than 150 ms. (Numbers for K^+ and Cl^- are in the same range.) If we conclude from the membrane voltage traces in Fig. 3 that the pore lifetime is shorter than 150 ms, say on the order of 10 ms, as a rough approximation, we still need only 15 pores to depolarize the membrane. For the very short pore lifetimes around 100 ns seen in simulations of simple phospholipid bilayers (not cell membranes) (Levine and Vernier 2012), about 1.4×10^6 pores would be required to discharge the membrane. Although we have at this time no solid method for determining electropore densities or total numbers experimentally, continuum pore models of electroporation predict that nanosecond pulses do indeed produce millions of nanometer-scale pores in cells of similar size (Son et al. 2014). These estimates are of course tentative and speculative, but they are specific enough to stimulate further efforts to improve both the models and the experimental efforts.

Calcium Transients After Subnanosecond Pulse Exposure

Subnanosecond pulse-induced increases in intracellular calcium concentration could come from influx of extracellular calcium through either the picosecond pulse-permeabilized membrane or voltage-activated calcium channels triggered by the permeabilization-driven depolarization, similar to what has been reported previously for adrenal chromaffin cells (Craviso et al. 2012), and possibly also through calcium-induced calcium release from intracellular stores (Semenov et al. 2013). It cannot be excluded that some or all of the calcium influx comes through calcium channels directly activated by the picosecond pulsed electric field, but it seems unlikely that a protein channel could be activated on this time scale.

Picosecond Permeabilizing Electric Fields

The molecular simulation results presented here provide a plausible physical mechanism for membrane permeabilization by subnanosecond stimuli—water intrusion and bridge formation, accompanied by phospholipid redistribution into the water defect regions. The apparent discrepancy between the somewhat larger fields employed in the MD simulations and the smaller fields used experimentally may be addressed in the following way. For a given transmembrane potential (or the corresponding applied electric field), there is a certain probability of lipid pore formation over a given area over a given time interval. This probability of pore formation increases *exponentially* with transmembrane voltage (applied field) (Vernier et al. 2013). Computational constraints on simulations of hydrated lipid bilayer systems with atomic resolution permit us to sample only a very small area compared to experimental observations. The membrane area for the simulations reported here (about 50 nm^2) represents a fraction of only 10^{-7} of the area of a typical cell membrane. This very small observational window means that to "see" an event that would produce thousands of pores in a cell, we must increase the probability of the event by a factor of several thousand (or run thousands of simulations), and we effectively accomplish that by increasing the applied field.

Thermal Effects

The possibility that the responses of cells (and membranes) to repetitive, high-field electric pulses are a consequence of temperature increases in the system must always be considered, especially when large numbers of pulses at high repetition rates are required to produce a given effect. Because the pulses are so few and so short, the total electric pulse energy in the experiments reported here, even if it were completely converted to heat, would increase the temperature of the exposed regions only by about 0.5 K with worst case assumptions. Simulation temperatures are regulated by a thermostat. Thus any temperature changes that may be occurring in the experiments or in the simulations are small and brief. However, we are adding energy, which results in a change in the properties of the cell membranes and lipid bilayers and a physical redistribution of their components. It may be instructive to think of this membrane electropermeabilization as a phase change, or a physical change of state, that is isothermal but which involves an increase in the energy of the system.

Summary

Subnanosecond ($\leq$500 ps) electric pulses activate rat hippocampal neurons and trigger calcium transients in NG108 rat neuroblastoma-glioma hybrid cells. Molecular simulations of phospholipid bilayers in electric fields show lipid electropore formation and membrane disorganization in less than 1 ns. Water dipoles in the membrane interior orient in permeabilizing electric fields on a picosecond time scale, consistent with a mechanism involving energy-minimizing intrusions of interfacial water leading to membrane permeabilization by picosecond electric pulses and terahertz electromagnetic fields.

Acknowledgments The study was supported in part by R21EB016912 from the National Institute of Biomedical Imaging and Bioengineering (SX and AP) and in part by the Air Force Office of Scientific Research (PTV). Computing resources were provided by the University of Southern California Center for High Performance Computing and Communications (http://www.usc.edu/hpcc/) and by the Turing High Performance Computing cluster at Old Dominion University (http://www.odu.edu/facultystaff/research/resources/computing/high-performance-computing).

References

Abidor IG, Arakelyan VB, Chernomordik LV, Chizmadzhev YA, Pastushenko VF, Tarasevich MR (1979) Electric breakdown of bilayer lipid membranes I. Main experimental facts and their qualitative discussion. Bioelectrochem Bioenerg 6:37–52

Albini M, Dinarelli S, Pennella F, Romeo S, Zampetti E, Girasole M, Morbiducci U, Massa R, Ramundo-Orlando A (2014) Induced movements of giant vesicles by millimeter wave radiation. Biochim Biophys Acta 1838:1710–1718

Barthel J, Bachhuber K, Buchner R, Hetzenauer H (1990) Dielectric spectra of some common solvents in the microwave region. Water and lower alcohols. Chem Phys Lett 165:369–373

Batista Napotnik T, Wu YH, Gundersen MA, Miklavcic D, Vernier PT (2012) Nanosecond electric pulses cause mitochondrial membrane permeabilization in Jurkat cells. Bioelectromagnetics 33:257–264

Benz R, Zimmermann U (1980) Pulse-length dependence of the electrical breakdown in lipid bilayer membranes. Biochim Biophys Acta 597:637–642

Bockmann RA, de Groot BL, Kakorin S, Neumann E, Grubmuller H (2008) Kinetics, statistics, and energetics of lipid membrane electroporation studied by molecular dynamics simulations. Biophys J 95:1837–1850

Buchner R, Barthel J, Stauber J (1999) The dielectric relaxation of water between 0 °C and 35 °C. Chem Phys Lett 306:57–63

Camp JT, Jing Y, Zhuang J, Kolb JF, Beebe SJ, Song JH, Joshi RP, Xiao S, Schoenbach KH (2012) Cell death induced by subnanosecond pulsed electric fields at elevated temperatures. IEEE Trans Plasma Sci 40:2334–2347

Chizmadzhev YA, Abidor IG (1980) Bilayer lipid membranes in strong electric fields. Bioelectrochem Bioenerg 7:83–100

Coster HGL (1965) A quantitative analysis of the voltage-current relationships of fixed charge membranes and the associated property of "punch-through". Biophys J 5:669–686

Craviso GL, Choe S, Chatterjee P, Chatterjee I, Vernier PT (2010) Nanosecond electric pulses: a novel stimulus for triggering Ca^{2+} influx into chromaffin cells via voltage-gated Ca^{2+} channels. Cell Mol Neurobiol 30:1259–1265

Craviso GL, Choe S, Chatterjee I, Vernier PT (2012) Modulation of intracellular Ca^{2+} levels in chromaffin cells by nanoelectropulses. Bioelectrochemistry 87:244–252

Frandsen SK, Gissel H, Hojman P, Tramm T, Eriksen J, Gehl J (2012) Direct therapeutic applications of calcium electroporation to effectively induce tumor necrosis. Cancer Res 72:1336–1341

Gowrishankar TR, Weaver JC (2003) An approach to electrical modeling of single and multiple cells. Proc Natl Acad Sci U S A 100:3203–3208

Gurtovenko AA, Vattulainen I (2005) Pore formation coupled to ion transport through lipid membranes as induced by transmembrane ionic charge imbalance: atomistic molecular dynamics study. J Am Chem Soc 127:17570–17571

Gurtovenko AA, Vattulainen I (2007) Ion leakage through transient water pores in protein-free lipid membranes driven by transmembrane ionic charge imbalance. Biophys J 92:1878–1890

Heller LC, Heller R (2006) In vivo electroporation for gene therapy. Hum Gene Ther 17:890–897

Hess B, Kutzner C, van der Spoel D, Lindahl E (2008) GROMACS 4: algorithms for highly efficient, load-balanced, and scalable molecular simulation. J Chem Theory Comput 4:435–447

Hille B (2001) Ion channels of excitable membranes, vol 507. Sinauer, Sunderland

Hintzsche H, Jastrow C, Heinen B, Baaske K, Kleine-Ostmann T, Schwerdtfeger M, Shakfa MK, Karst U, Koch M, Schrader T, Stopper H (2013) Terahertz radiation at 0.380 THz and 2.520 THz does not lead to DNA damage in skin cells in vitro. Radiat Res 179:38–45

Ho MC, Casciola M, Levine ZA, Vernier PT (2013) Molecular dynamics simulations of ion conductance in field-stabilized nanoscale lipid electropores. J Phys Chem B 117:11633–11640

Humphrey W, Dalke A, Schulten K (1996) VMD: visual molecular dynamics. J Mol Graph 14(33–8):27–28

Ibey BL, Mixon DG, Payne JA, Bowman A, Sickendick K, Wilmink GJ, Roach WP, Pakhomov AG (2010) Plasma membrane permeabilization by trains of ultrashort electric pulses. Bioelectrochemistry 79:114–121

Ibey BL, Roth CC, Pakhomov AG, Bernhard JA, Wilmink GJ, Pakhomova ON (2011) Dose-dependent thresholds of 10-ns electric pulse induced plasma membrane disruption and cytotoxicity in multiple cell lines. PLoS ONE 6:e15642

Kim KT, Park J, Jo SJ, Jung S, Kwon OS, Gallerano GP, Park WY, Park GS (2013) High-power femtosecond-terahertz pulse induces a wound response in mouse skin. Sci Rep 3:2296

Koronkiewicz S, Kalinowski S, Bryl K (2002) Programmable chronopotentiometry as a tool for the study of electroporation and resealing of pores in bilayer lipid membranes. Biochim Biophys Acta 1561:222–229

Kotnik T, Miklavcic D (2000) Second-order model of membrane electric field induced by alternating external electric fields. IEEE Trans Biomed Eng 47:1074–1081

Levine ZA, Vernier PT (2010) Life cycle of an electropore: field-dependent and field-independent steps in pore creation and annihilation. J Membr Biol 236:27–36

Levine ZA, Vernier PT (2012) Calcium and phosphatidylserine inhibit lipid electropore formation and reduce pore lifetime. J Membr Biol 245:599–610

Marrink SJ, de Vries AH, Tieleman DP (2009) Lipids on the move: simulations of membrane pores, domains, stalks and curves. Biochim Biophys Acta 1788:149–168

Marty M, Sersa G, Garbay JR, Gehl J, Collins CG, Snoj M, Billard V, Geertsen PF, Larkin JO, Miklavcic D, Pavlovic I, Paulin-Kosir SM, Cemazar M, Morsli N, Rudolf Z, Robert C, O'Sullivan GC, Mir LM (2006) Electrochemotherapy-easy, highly effective and safe treatment of cutaneous and subcutaneous metastases: results of ESOPE (European Standard Operating Procedures of Electrochemotherapy) study. Eur J Cancer Suppl 4:3–13

Melikov KC, Frolov VA, Shcherbakov A, Samsonov AV, Chizmadzhev YA, Chernomordik LV (2001) Voltage-induced nonconductive pre-pores and metastable single pores in unmodified planar lipid bilayer. Biophys J 80:1829–1836

Napotnik TB, Rebersek M, Kotnik T, Lebrasseur E, Cabodevila G, Miklavcic D (2010) Electropermeabilization of endocytotic vesicles in B16 F1 mouse melanoma cells. Med Biol Eng Comput 48:407–413

Naumowicz M, Figaszewski ZA (2013) Pore formation in lipid bilayer membranes made of phosphatidylcholine and cholesterol followed by means of constant current. Cell Biochem Biophys 66:109–119

Nesin OM, Pakhomova ON, Xiao S, Pakhomov AG (2010) Manipulation of cell volume and membrane pore comparison following single cell permeabilization with 60- and 600-ns electric pulses. Biochim Biophys Acta 1808:792–801

Neu JC, Krassowska W (1999) Asymptotic model of electroporation. Phys Rev E 59:3471–3482

Neumann E, Schaefer-Ridder M, Wang Y, Hofschneider PH (1982) Gene transfer into mouse lyoma cells by electroporation in high electric fields. EMBO J 1:841–845

Nuccitelli R, Pliquett U, Chen X, Ford W, Swanson RJ, Beebe SJ, Kolb JF, Schoenbach KH (2006) Nanosecond pulsed electric fields cause melanomas to self-destruct. Biochem Biophys Res Commun 343:351–360

Pakhomov AG, Kolb JF, White JA, Joshi RP, Xiao S, Schoenbach KH (2007a) Long-lasting plasma membrane permeabilization in mammalian cells by nanosecond pulsed electric field (nsPEF). Bioelectromagnetics 28:655–663

Pakhomov AG, Shevin R, White JA, Kolb JF, Pakhomova ON, Joshi RP, Schoenbach KH (2007b) Membrane permeabilization and cell damage by ultrashort electric field shocks. Arch Biochem Biophys 465:109–118

Pakhomov AG, Bowman AM, Ibey BL, Andre FM, Pakhomova ON, Schoenbach KH (2009) Lipid nanopores can form a stable, ion channel-like conduction pathway in cell membrane. Biochem Biophys Res Commun 385:181–186

Pakhomova ON, Khorokhorina VA, Bowman AM, Rodaite-Riseviciene R, Saulis G, Xiao S, Pakhomov AG (2012) Oxidative effects of nanosecond pulsed electric field exposure in cells and cell-free media. Arch Biochem Biophys 527:55–64

Pal S, Balasubramanian S, Bagchi B (2004) Anomalous dielectric relaxation of water molecules at the surface of an aqueous micelle. J Chem Phys 120:1912–1920

Ramundo-Orlando A, Gallerano GP (2009) Terahertz radiation effects and biological applications. J Infrared Millim Terahertz Waves 30:1308–1318

Ramundo-Orlando A, Gallerano GP, Stano P, Doria A, Giovenale E, Messina G, Cappelli M, D'Arienzo M, Spassovsky I (2007) Permeability changes induced by 130 GHz pulsed radiation on cationic liposomes loaded with carbonic anhydrase. Bioelectromagnetics 28:587–598

Rols MP (2006) Electropermeabilization, a physical method for the delivery of therapeutic molecules into cells. Biochim Biophys Acta 1758:423–428

Romanenko S, Siegel PH, Wagenaar DA, Pikov V (2014) Effects of millimeter wave irradiation and equivalent thermal heating on the activity of individual neurons in the leech ganglion. J Neurophysiol 112:2423–2431

Romeo S, Wu YH, Levine ZA, Gundersen MA, Vernier PT (2013) Water influx and cell swelling after nanosecond electropermeabilization. Biochim Biophys Acta 1828:1715–1722

Schoenbach KH, Beebe SJ, Buescher ES (2001) Intracellular effect of ultrashort electrical pulses. Bioelectromagnetics 22:440–448

Schoenbach KH, Xiao S, Joshi RP, Camp JT, Heeren T, Kolb JF, Beebe SJ (2008) The effect of intense subnanosecond electrical pulses on biological cells. IEEE Trans Plasma Sci 36:414–422

Semenov I, Xiao S, Pakhomov AG (2013) Primary pathways of intracellular Ca^{2+} mobilization by nanosecond pulsed electric field. Biochim Biophys Acta 1828:981–989

Silve A, Leray I, Mir LM (2012) Demonstration of cell membrane permeabilization to medium-sized molecules caused by a single 10 ns electric pulse. Bioelectrochemistry 87:260–264

Son RS, Smith KC, Gowrishankar TR, Vernier PT, Weaver JC (2014) Basic features of a cell electroporation model: illustrative behavior for two very different pulses. J Membr Biol 247:1209–1228

Sterpone F, Marchetti G, Pierleoni C, Marchi M (2006) Molecular modeling and simulation of water near model micelles: diffusion, rotational relaxation and structure at the hydration interface. J Phys Chem B 110:11504–11510

Sugar IP, Neumann E (1984) Stochastic model for electric field-induced membrane pores. Electroporation Biophys Chem 19:211–225

Tarek M (2005) Membrane electroporation: a molecular dynamics simulation. Biophys J 88:4045–4053

Teissie J, Rols MP (1993) An experimental evaluation of the critical potential difference inducing cell membrane electropermeabilization. Biophys J 65:409–413

Teissie J, Golzio M, Rols MP (2005) Mechanisms of cell membrane electropermeabilization: a minireview of our present (lack of ?) knowledge. Biochim Biophys Acta 1724:270–280

Tekle E, Oubrahim H, Dzekunov SM, Kolb JF, Schoenbach KH, Chock PB (2005) Selective field effects on intracellular vacuoles and vesicle membranes with nanosecond electric pulses. Biophys J 89:274–284

Tieleman DP (2004) The molecular basis of electroporation. BMC Biochem 5:10

Tielrooij KJ, Paparo D, Piatkowski L, Bakker HJ, Bonn M (2009) Dielectric relaxation dynamics of water in model membranes probed by terahertz spectroscopy. Biophys J 97:2484–2492

Timoshkin IV, MacGregor SJ, Fouracre RA, Crichton BH, Anderson JG (2006) Transient electrical field across cellular membranes: pulsed electric field treatment of microbial cells. J Phys D 39:596–603

Titova LV, Ayesheshim AK, Golubov A, Fogen D, Rodriguez-Juarez R, Hegmann FA, Kovalchuk O (2013a) Intense THz pulses cause H2AX phosphorylation and activate DNA damage response in human skin tissue. Biomed Opt Express 4:559–568

Titova LV, Ayesheshim AK, Golubov A, Rodriguez-Juarez R, Woycicki R, Hegmann FA, Kovalchuk O (2013b) Intense THz pulses down-regulate genes associated with skin cancer and psoriasis: a new therapeutic avenue? Sci Rep 3:2363

Tokman M, Lee JH, Levine ZA, Ho MC, Colvin ME, Vernier PT (2013) Electric field-driven water dipoles: nanoscale architecture of electroporation. PLoS ONE 8:e61111

Tolstykh GP, Beier HT, Roth CC, Thompson GL, Ibey BL (2014) 600 ns pulse electric field-induced phosphatidylinositol$_{4,5}$-bisphosphate depletion. Bioelectrochemistry 100:80–87

Vernier PT, Sun Y, Marcu L, Salemi S, Craft CM, Gundersen MA (2003) Calcium bursts induced by nanosecond electric pulses. Biochem Biophys Res Commun 310:286–295

Vernier PT, Sun Y, Marcu L, Craft CM, Gundersen MA (2004) Nanosecond pulsed electric fields perturb membrane phospholipids in T lymphoblasts. FEBS Lett 572:103–108

Vernier PT, Sun Y, Gundersen MA (2006a) Nanoelectropulse-driven membrane perturbation and small molecule permeabilization. BMC Cell Biology 7:37

Vernier PT, Ziegler MJ, Sun Y, Gundersen MA, Tieleman DP (2006b) Nanopore-facilitated, voltage-driven phosphatidylserine translocation in lipid bilayers - in cells and in silico. Phys Biol 3:233–247

Vernier PT, Levine ZA, Gundersen MA (2013) Water bridges in electropermeabilized phospholipid bilayers. Proc IEEE 101:494–504

Weaver JC, Chizmadzhev YA (1996) Theory of electroporation: a review. Bioelectrochem Bioenerg 41:135–160

Williams R, Schofield A, Holder G, Downes J, Edgar D, Harrison P, Siggel-King M, Surman M, Dunning D, Hill S, Holder D, Jackson F, Jones J, McKenzie J, Saveliev Y, Thomsen N, Williams P, Weightman P (2013) The influence of high intensity terahertz radiation on mammalian cell adhesion, proliferation and differentiation. Phys Med Biol 58:373–391

Wilmink GJ, Rivest BD, Roth CC, Ibey BL, Payne JA, Cundin LX, Grundt JE, Peralta X, Mixon DG, Roach WP (2011) In vitro investigation of the biological effects associated with human

dermal fibroblasts exposed to 2.52 THz radiation. Lasers Surg Med 43:152–163

Xiao S, Guo S, Nesin V, Heller R, Schoenbach KH (2011) Subnanosecond electric pulses cause membrane permeabilization and cell death. IEEE Trans Biomed Eng 58:1239–1245

Zeni O, Gallerano GP, Perrotta A, Romano M, Sannino A, Sarti M, D'Arienzo M, Doria A, Giovenale E, Lai A, Messina G, Scarfi MR (2007) Cytogenetic observations in human peripheral blood leukocytes following in vitro exposure to THz radiation: a pilot study. Health Phys 92:349–357

Zimmermann U, Pilwat G, Riemann F (1974) Dielectric breakdown of cell membranes. Biophys J 14:881–899